Journal of ELECTRONIC MATERIALS, Vol. 45, No. 4, 2016
DOI: 10.1007/s11664-015-4252-0

Influence of Processing Conditions and Material Properties on Electrohydrodynamic Direct Patterning of a Polymer Solution

SHIN JANG,[1] YEONGJUN KIM,[1] and JE HOON OH[1,2]

1.—Department of Mechanical Engineering, Hanyang University, 55 Hanyangdaehak-ro, Sangrok-gu, Ansan, Gyeonggi-do 426-791, Korea. 2.—e-mail: jehoon@hanyang.ac.kr

An electrohydrodynamic (EHD) patterning method was utilized to obtain high-resolution line patterns in a low electric field regime without an additional mechanical drawing process. Molecular weight and weight percent of a polymer were selected as key parameters to reduce the voltage. EHD patterning was performed using polyethylene oxide (PEO) solutions. The threshold voltages (V_{th}) to initiate jet ejection are almost the same for all solutions. A method verified in this study, reducing the driving voltage (V_d) just after the initiation of the jet at the threshold voltage, can make a very thin, continuous jet, while increasing molecular weight and weight percent were enabled to further reduce the input voltage. As the voltage reduction ratio (V_d/V_{th}) is decreased, the jet behaves like a solid rather than a liquid due to its fast solidification. The line width of the resultant line pattern could be tuned from 50 nm to 10 μm depending on the substrate moving speed. Contour maps were also developed that show the pattern mode variation as a function of the voltage reduction ratio and key parameters. The results show that well-defined PEO line and grid patterns can be fabricated via the proposed EHD direct patterning under appropriate conditions.

Key words: Electrohydrodynamic patterning, polyethylene oxide (PEO) solution, threshold voltage, molecular weight, electrospinning

INTRODUCTION

Polymers have been widely used in various printed electronics fields such as conductors,[1–3] organic thin film transistors,[4,5] nanogenerators,[6,7] capacitive sensors,[8] bio-sensors,[9] membrane filters,[10] and bio-medical applications.[11,12] They are ideally suited for flexible, bendable, stretchable and transparent applications due to their mechanical and electrical characteristics. To facilitate the development of such applications using polymers, solution-based manufacturing technologies are now more preferred over the conventional technologies that commonly require high-temperature and vacuum-based processes, because the polymers are sensitive to thermal damage. Among these solution-based technologies, inkjet printing has been regarded as a highly cost-effective, flexible, and eco-friendly process; however, it is limited to solutions with low viscosity and surface tension, suggesting that thick polymer solutions are not compatible with this technology. Moreover, limited resolution dependent on nozzle diameter is also a significant problem in the inkjet printing; thus, the nozzle diameter should be reduced to improve the printing resolution. However, this may give rise to other problems including nozzle clogging as well as a high manufacturing cost.[13,14] Recently, electrohydrodynamic (EHD) direct patterning methods[15–19] have been suggested for printing thick solutions on demand with high resolutions by reducing the input voltage and gap distance between the nozzle tip and the ground electrode.

EHD direct patterning is based on typical electrospinning.[20–23] In the electrospinning, a solution is extracted from the orifice of a spinneret via the application of an electric potential between the spinneret and a ground electrode. After the positive

(Received July 15, 2015; accepted November 13, 2015; published online December 9, 2015)

voltage is applied to the spinneret, negative and positive charges are separated within the solution, and then the positive charges are distributed on the surface of a meniscus, leading to the generation of electric forces between the surface and the ground electrode (Fig. 1). The meniscus of the solution is then deformed into a cone shape, and once the summation of the electric and hydrostatic forces exceeds the surface tension of the solution, a jet is ejected from the apex of the cone. Since the ejected jet still contains positively-charged ions, which cause strong repulsive forces and local electric fields, a bending of the jet, known as bending (or whipping) instability, is initiated, resulting in the jets being randomly distributed on a substrate (or a collector).

While polymer fibers are randomly distributed in typical electrospinning, EHD direct patterning is able to print a solution more precisely by suppressing such instabilities. Moreover, high-resolution patterning is possible since the size of the jet can be significantly smaller than the inner diameter of the nozzle. To achieve high-resolution and accurate EHD direct patterning, it is crucial to consider the key factors such as the solution property, the distance between the nozzle and the ground electrode, and control of the electric potential. Hellmann et al. conducted EHD direct patterning by significantly reducing the distance between the nozzle and the substrate, but some instabilities were still evident due to the relatively high electric potential used in their investigation.[15] For the purpose of further reducing instabilities, Chang et al. introduced a mechanical drawing process with a micro-tip to stimulate the solution meniscus, and was able make a single nanofiber with a diameter of ~40 nm.[16] However, micro-tipping the meniscus should be done very precisely and might cause electric shocks due to the high electric field, 1.2×10^6 V/m, which could lead to unwanted jet behaviors and pattern formation. Therefore, high-resolution patterning at extremely low electric fields is preferred for EHD direct patterning. However, a systematic approach and methodology for high-resolution EHD direct patterning without any mechanical assistance has yet to be clearly established.

In this study, we introduced a simple approach based on a EHD patterning method to produce a single nanofiber of 50 nm diameter at a low electric field, $\sim 0.2 \times 10^6$ V/m, without using any mechanical assistance. Molecular weight and weight percent, voltage reduction ratio, and stage motion were adopted as key parameters and EHD direct patterning using a polyethylene oxide (PEO) solution was systematically investigated from jet initiation to deposition, both with and without stage motion. The threshold voltage required to exceed the surface tension force was examined by varying the solution properties such as molecular weights and weight percentages of PEO. The effects of the voltage reduction ratio on jet behavior were then demonstrated by gradually decreasing the driving voltage from the threshold voltage. Then, PEO jets were printed onto an indium tin oxide (ITO)-coated glass to study the effects of stage motion, and contour maps were generated to show how the resultant patterns varied with different solution properties and electric potentials. Finally, various patterns including line arrays and grids were fabricated to demonstrate the feasibility of the patterning method.

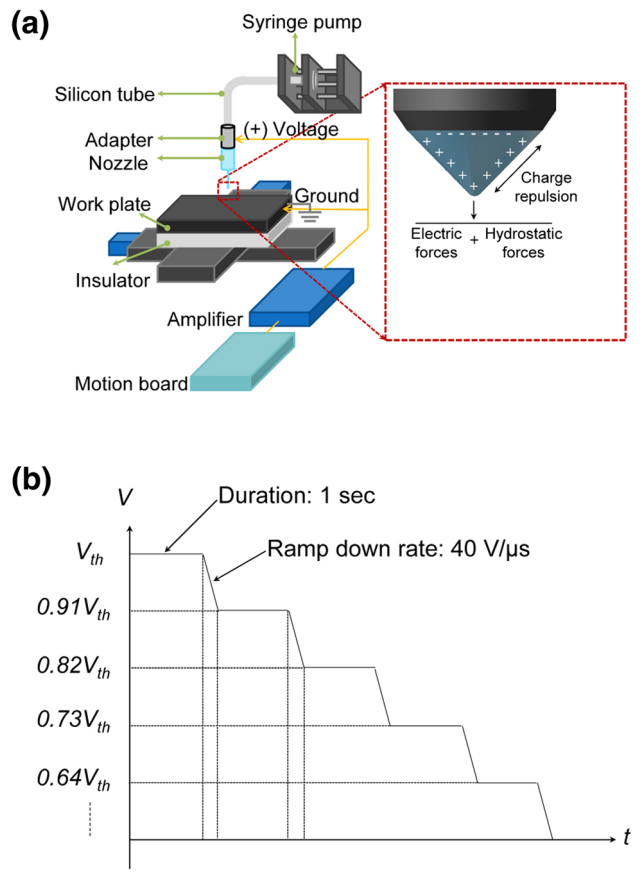

Fig. 1. (a) Schematic illustration of the in-house EHD direct patterning system and the mechanism of jet formation. (b) Input voltage profile when adjusting the voltage reduction ratio (*R*).

MATERIALS AND METHODS

PEO was used as a patterning solution in this work because it is soluble in water and the property of solution is relatively easily adjusted. PEO powders with three different viscosity-averaged molecular weights (M_v: 20×10^4, 40×10^4 and 60×10^4) were purchased from Sigma Aldrich and dissolved in deionized (DI) water for 24 h using a magnetic stirrer. A total of nine PEO solutions were then prepared with 2 wt.%, 4 wt.%, and 6 wt.% for each molecular weight.

EHD direct patterning experiments were performed with an in-house system as illustrated in

Fig. 1a. A nozzle (32 G) with inner diameter of ~100 μm was connected to an adaptor that acted as an upper electrode, and a voltage amplifier was used to apply high electric potentials to the solution. ITO-coated glass with 1.1 mm thickness was used as a substrate and placed on the ground electrode connected to the motorized X–Y moving stage controlled by servo motors. This ITO-coated glass was ultrasonicated in deionized water for 15 min to remove surface contamination. For all experiments, the distance between the nozzle tip and the top surface of the ITO-coated glass was fixed at 2 mm, and PEO solutions were fed into the nozzle using a syringe pump (Harvard) at a flow rate of 0.05 μL/min. The driving voltage (V_d) was increased up to a threshold voltage (V_{th}) and then was gradually decreased in order to study the effects of the voltage reduction ratio (R) on the jet behaviors and the resulting patterns and to eventually obtain stable and fine jets. V_{th} was defined as the voltage at which jet ejection is initiated while increasing V_d, and R was defined as the ratio of V_d to V_{th} ($R = V_d/V_{th}$) when decreasing V_d from V_{th}. It should be noted that R is always less than 1.

When adjusting R, the ramp down rate of the driving voltage used in our experiments was 40 V/μs and its effect was not strong. However, a jet was sometimes not continuously ejected for the solutions with low molecular weight and PEO concentration when the driving voltage was abruptly reduced from V_{th} to V_d with a preset R. Therefore, we used the programmed step profile for the voltage when adjusting R, as shown in Fig. 1b.

Solution properties such as viscosity and surface tension were measured using a viscometer (Brookfield) and surface tension analyzer (SEO), respectively. A CCD camera (Sony) equipped with an optical zoom lens was used to observe the jet behaviors. An optical microscope (Olympus) and a field emission scanning electron microscope (FE-SEM; Hitachi) were used to characterize the printed patterns and microstructures, respectively.

RESULTS AND DISCUSSION

Solution properties were characterized prior to conducting the EHD direct patterning. Figure 2 shows the surface tension and viscosity of nine PEO solutions with various M_v and wt.% of the PEO. As the M_v and wt.% are increased, the surface tension of the solution is slightly decreased since the PEO is known to be surface active at the air–water interface. The high M_v and wt.% of the PEO slightly improved the surface activity of the solution.[24] On the other hand, apparent variation was observed for the viscosity, as expected. High M_v and wt.% lead to a strong viscous effect, resulting in 10–100 times higher viscosity values.

EHD direct patterning experiments were performed to investigate the jet behaviors of nine PEO solutions. V_{th}, required to initiate jet ejection, was

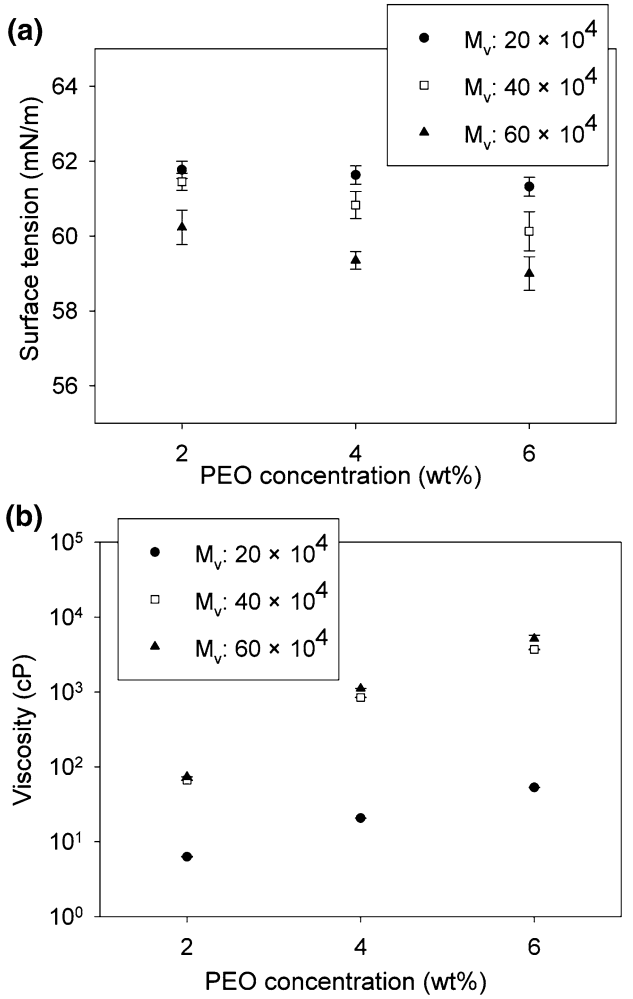

Fig. 2. Variation of (a) the surface tension and (b) the viscosity of PEO solutions with different molecular weights and weight percents.

measured for each solution, as shown in Fig. 3a. V_{th} is not very different for each solution and ranged from 2.1 kV to 2.2 kV. In EHD direct patterning, jet ejection is governed by surface tension, electric field, and hydrostatic forces as follows:

$$\frac{2\sigma}{r} < \frac{1}{2}\varepsilon E^2 + \rho g h \qquad (1)$$

where σ is the surface tension of the solution, r the radius of curvature of the solution meniscus, ε the electric permittivity of air, E the electric field exerted by the driving voltage, ρ the density of a solution, g the gravitational acceleration, and h the height of the solution in the nozzle. If the summation of the electric field and hydrostatic forces exceeds the surface tension force, a jet is ejected from the apex of the Taylor cone. Due to the similar σ of each solution, V_{th} becomes similar (Fig. 3a).

As V_d is increased, the liquid meniscus expands before reaching V_{th}, and a jet with relatively strong instability is finally ejected at the V_{th} (Fig. 3b). The

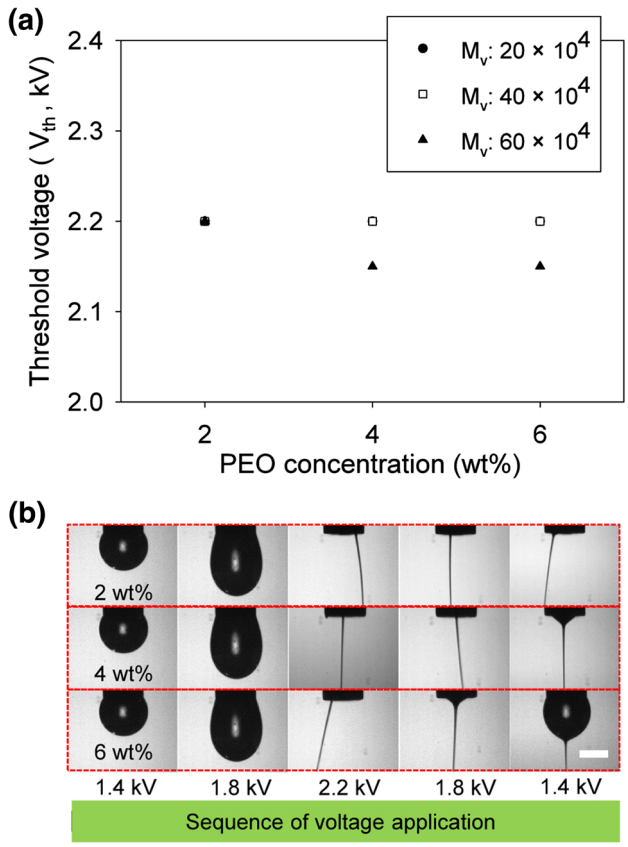

Fig. 3. (a) Effect of M_v and wt.% on the threshold voltage (V_{th}) for jet initiation, and (b) effect of the change of driving voltage (V_d) on jet behaviors of the PEO ($M_v = 60 \times 10^4$) solutions with different PEO contents. Scale bar 100 μm.

jet instability becomes more severe and even an electrical breakdown occurs at V_d higher than V_{th}, so higher V_d should be avoided to obtain stable, fine jets. Instead, it was observed that once a jet is initiated at V_{th}, the jet can be continuously ejected without breakup even when V_d is gradually decreased from V_{th}. It was also found that this phenomenon is influenced by the solution property which depends on M_v and wt.%.

In order to investigate the effects of M_v and wt.% on the jet behaviors of PEO solutions while V_d is reduced from V_{th}, the jet behaviors of all the PEO solutions were observed by varying R. Figure 4 illustrates the jet behaviors of PEO solutions with different M_v and wt.% at various values of R. For the PEO solutions of 2 wt.%, the jets are sprayed until $R = 0.82$ and then are not ejected below $R = 0.64$ when $M_v = 20 \times 10^4$. Although continuous jets are observed at $R = 0.64$ when $M_v = 40 \times 10^4$ and 60×10^4, they look unstable. At lower R, the jet is not ejected regardless of M_v (Fig. 4a).

When the PEO concentration is increased to 4 wt.%, continuous jets are observed at a further decreased R of 0.45 for $M_v = 40 \times 10^4$ and 60×10^4 (Fig. 4b). This is likely due to the contribution of the increased viscoelastic properties of the solution. During the ejection, the jet becomes thin, which implies that the solvent is easily evaporated, accelerating the reduction in the jet diameter. The tensile stress acting on the jet then becomes large, and this, in turn, enhances the viscoelasticity of the jet. As a result, continuous jets are possible without breakup at $R = 0.45$. Note that there is no jet ejection at $R = 0.27$ for the 4 wt.% PEO solution.

It is interesting to mention that R can be further reduced to 0.27, corresponding to an electric field of 0.2×10^6 V/m, for the 6 wt.% PEO solution with $M_v = 60 \times 10^4$, leading to the thinnest jet ejection from the nozzle, despite a large meniscus due to a weak electric field and strong viscosity (Fig. 4c). If R becomes less than 0.27, the jet ejection stops, while the meniscus becomes larger and is dropped onto the substrate or climbs up the outer wall of the nozzle, terminating the jet ejection. From this experimental result, it was found that the jet ejection behavior for all the solutions investigated is similar at higher R, but wt.% and M_v should be increased to obtain a thinner jet at lower R. The thinnest jet was generated at $R = 0.27$ for the 6 wt.% PEO solution with $M_v = 60 \times 10^4$.

The jet behaviors almost determine the size and shape of the patterns printed on a substrate. Figure 5a–c presents the jet behavior near the nozzle, the jet deposition near the substrate and the resultant pattern, respectively, for the 6 wt.% PEO solution with $M_v = 60 \times 10^4$ at $R = 0.64$ when the substrate is stationary. Figure 5d–f are for the same solution at $R = 0.45$. The size of the jet at $R = 0.64$ is larger than that at $R = 0.45$. While the jet driven by $R = 0.64$ remains in the liquid phase when it reaches the substrate (Fig. 5b), the jet driven by $R = 0.45$ is nearly solidified because of the rapid evaporation, resulting in stacked nanofibers (Fig. 5e). In addition, when $R = 0.45$, weak buckling of the jet along the entire jet length is observed since the jet behaves like a column under compressive force. This buckling should be distinguished from the bending instability in typical electrospinning and can disappear on a moving substrate.

The inset SEM images in Fig. 5c and f represent the microstructures of the resultant patterns. Different R values generate quite different microstructures. While the pattern printed at $R = 0.64$ seems to be a PEO film, nanofiber webs are produced on the substrate at $R = 0.45$. Since the speed and size of the jet ejected at high R are relatively fast and large, the solvent is not likely to evaporate during the jet deposition, leading to the spreading of the PEO solution on the substrate. However, if R is further lowered, the solvent of the jet evaporates before reaching the substrate and, consequently, solid nanofibers are formed on the substrate. Jet instability is little observed as compared with typical electrospinning due to a relatively short gap distance and weak electric potential. A jet reaches the substrate before bending instability occurs, and the charges existing in the jet are also

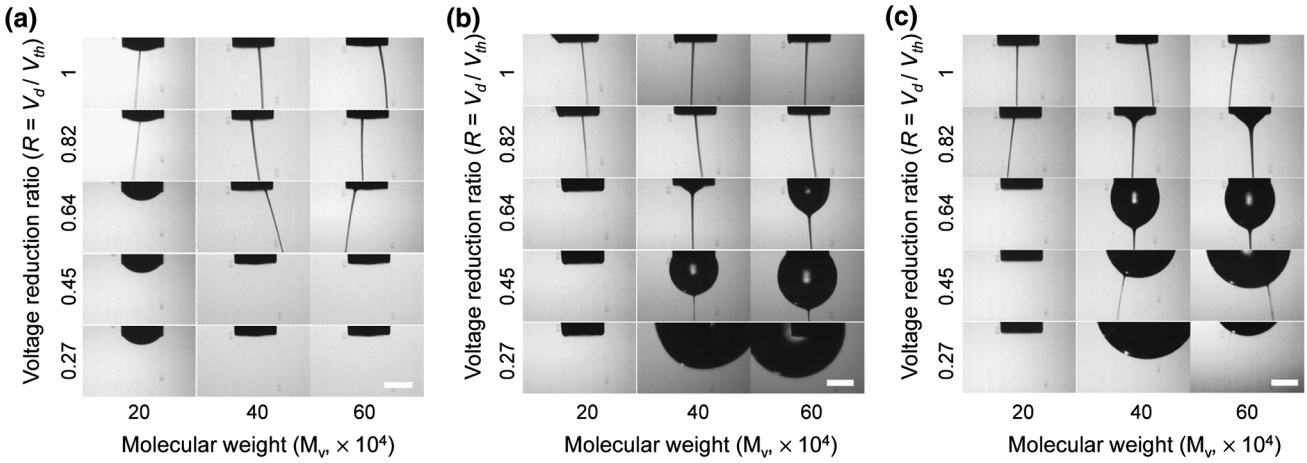

Fig. 4. Jet behaviors of the (a) 2 wt.%, (b) 4 wt.%, and (c) 6 wt.% PEO solutions with respect to M_v and R. Scale bar 100 μm.

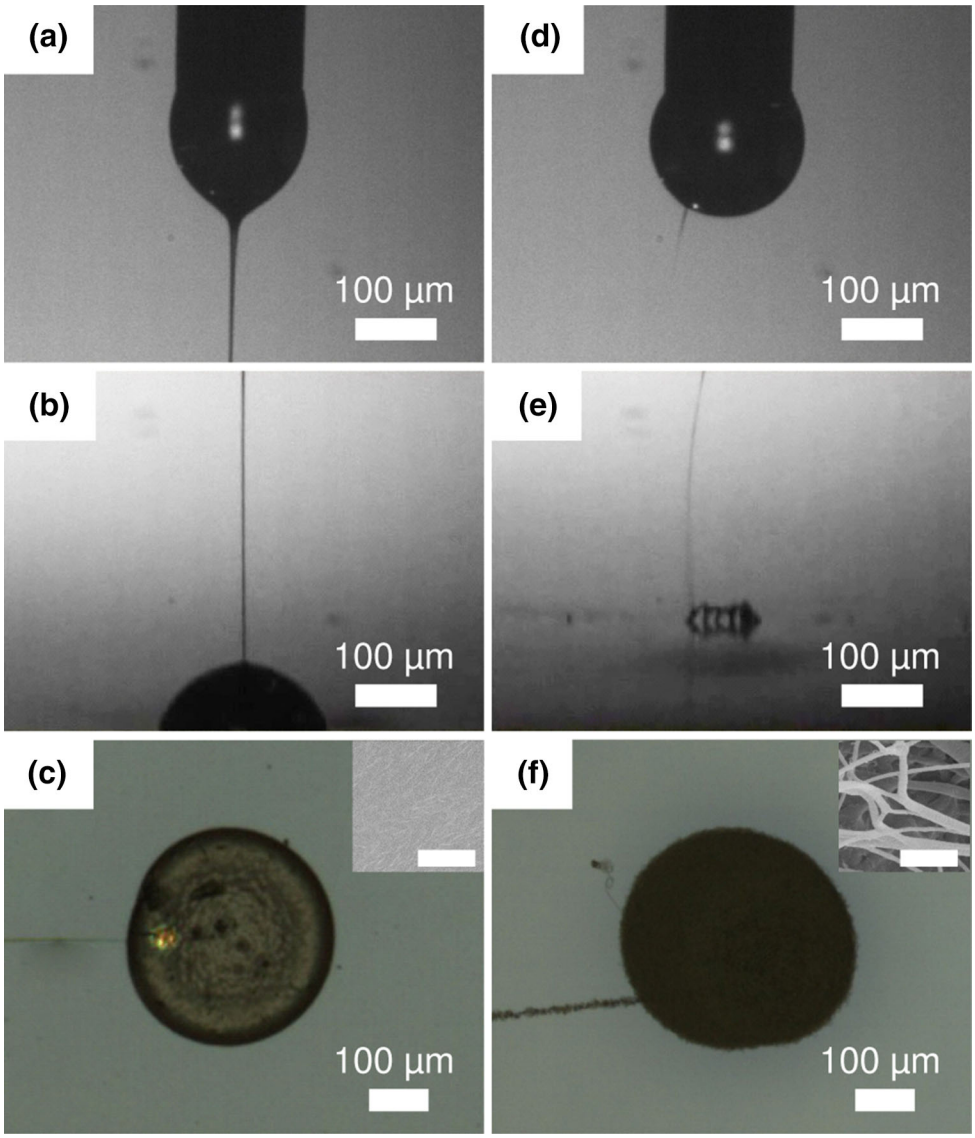

Fig. 5. Jet behaviors, jet deposition shapes, and resultant patterns on the stationary substrate for the 6 wt.% PEO (M_v = 60 × 10^4) solution at two different R values: (a–c) R = 0.64 and (d–f) R = 0.45. Scale bars in the insets of (c) and (f) are 100 nm.

easily neutralized on the substrate surface because of the small amount of the jet, which can also suppress bending instability.

EHD line patterning was conducted on the moving substrates at various stage speeds in order to examine the effect of substrate motion on the PEO line formation when the solution contained 6 wt.% PEO with $M_v = 60 \times 10^4$. The PEO solution was printed on substrates moving at 50 mm/s, 150 mm/s and 250 mm/s. Figure 6a shows the microscopic images as well as the SEM images of printed PEO lines for various stage speeds and R. For all the stage speeds, the line width decreases with decreasing the R. Similarly, for all the values of R, the line width decreases with increasing the stage speed. At the relatively low stage speed of 50 mm/s, the bead-on-string shapes (line bulges) are formed at an R value larger than 0.64. It is also interesting to note that, below $R = 0.45$, the buckling of the line occurs instead of the bead-on-string phenomenon. This verifies the fact that the jet is solidified before reaching the substrate at a low R due to the rapid evaporation of the solvent (also see the insets) since the buckling is caused by high compressive stress acting on a solid fiber. The buckling of the line becomes more severe at $R = 0.27$ because the compressive stress becomes higher due to the reduced cross-sectional area of the jet. In contrast, the slow evaporation at a high R makes the jet still liquid on the substrate, and the jet speed is faster than the stage speed; therefore, the bead-on-string shapes appear on the printed lines. As the stage speed increases, the bead-on-string phenomenon and the line buckling disappear, resulting in straight, uniform lines. In addition, from the inset SEM images, the jet is found to be spread on the substrate above $R = 0.64$. As shown in Fig. 6b, the width of the printed lines ranges from 50 nm to 1 μm depending on the R and stage speed. It should be noted that line widths of several tens of nm can be generated by the combination of the low R and high stage speed without any mechanical drawing process.

The patterning results obtained for different parameters at the stage speed of 150 mm/s are also plotted as a contour map in Fig. 7. This contour map shows how the pattern shape changes with respect to wt.%, M_v and R. The resultant patterns are classified into six modes based on the microscopic and SEM images: no jetting, spraying, bead-on-string, micro-pattern (spreading), nano-pattern (spreading), and nanofiber. For the 2 wt.% PEO solution, the jet with low M_v is sprayed at high R, but the bead-on-string line patterns occur with increased M_v. If R becomes lower, there is no jetting for all the values of M_v (Fig. 7a). The viscosity of the solution is low and the jet size is relatively large, so the evaporation rate is slow. Therefore, large beads are observed for the line pattern.

When the solution contains 4 wt.% of PEO, the spraying region disappears, the bead size is reduced, and micro- and nano-patterning regions

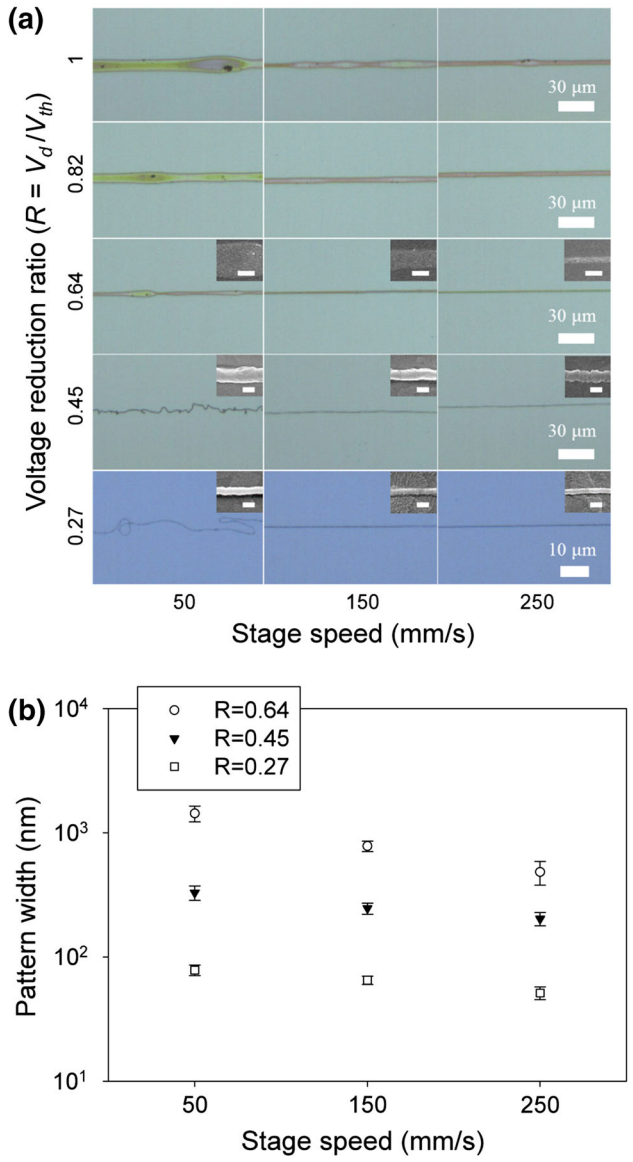

Fig. 6. (a) Effect of R and stage speed on the line pattern formation and (b) variation of the pattern width with R and the stage speed when the solution contains 6 wt.% PEO ($M_v = 60 \times 10^4$). Scale bars in the insets are 500 nm at $R = 0.64$ and 50 nm at $R = 0.45$ and 0.27.

are generated for the higher M_v and lower R (Fig. 7b). Due to spreading on the substrate during EHD patterning, the nano-pattern has several hundreds of nm width even at a low R. However, if the concentration of PEO is further increased to 6 wt.%, nanofibers whose widths are less than 100 nm can be formed because of rapid solidification before reaching the substrate (Fig. 7c). At higher concentration, the transition of the pattern mode occurs from beads-on-string to micro-patterns to nano-patterns to nanofibers as R is reduced.

Figure 8 shows the line arrays and grid patterns fabricated on the substrate when the 6 wt.% PEO solution with $M_v = 60 \times 10^4$ was EHD-printed at

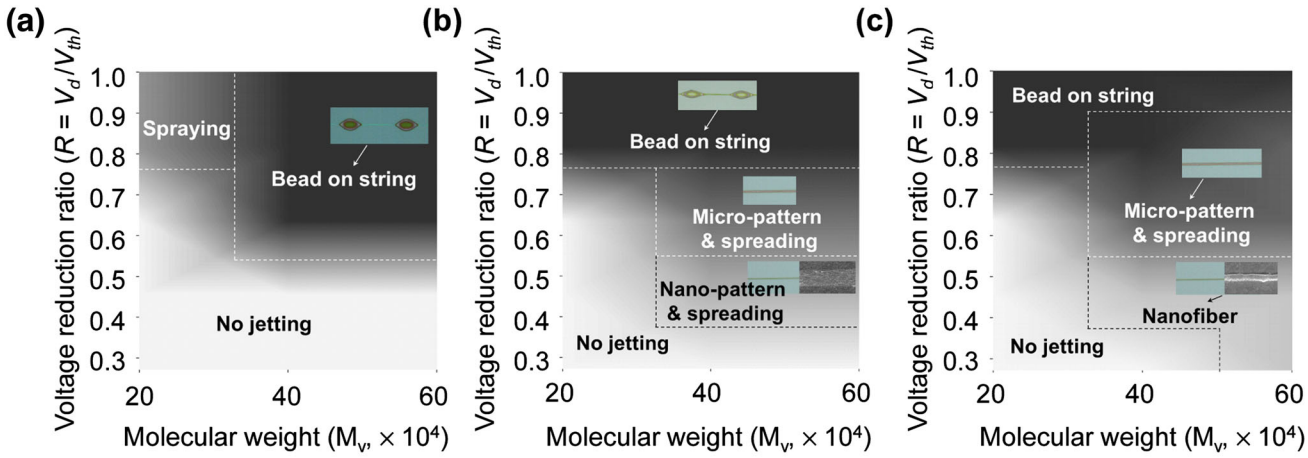

Fig. 7. Contour maps for resultant patterns with regard to R and M_v for the (a) 2 wt.%, (b) 4 wt.%, and (c) 6 wt.% PEO solutions.

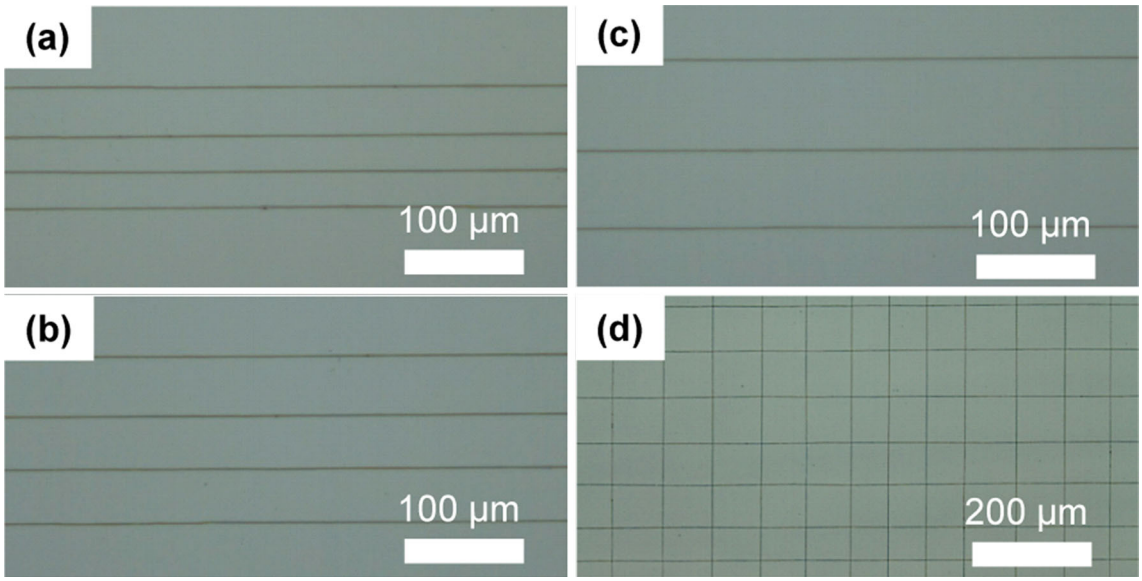

Fig. 8. (a–c) Line array patterns of the 6 wt.% PEO ($M_v = 60 \times 10^4$) solution with the line-to-line distance of 20 μm, 40 μm, and 80 μm, respectively. (d) Grid pattern with the grid size of 80 μm.

R = 0.27. The line arrays with a line-to-line distance of 20 μm, 40 μm and 80 μm are presented in Fig. 8-a–c, respectively. Well-defined and straight line arrays are fabricated on the ITO-coated glass. The grid pattern is also well obtained as shown in Fig. 8d, even though there was some deviation in the line spacing. The distance between the lines was measured as 80 $\pm$ 11 μm. It is known that line spacing errors in EHD pattering are attributed to reasons such as mechanical buckling and interference between the remaining charges in a jet and the external electric field.[20,25,26] A jet from the nozzle contains charges generating a local electric field which interferes with the external electric field, and this could make a deviation of the pattern from its desired position. The mechanical buckling of the jet and the fast stage motion could also lead to the position error. Therefore, such deviation of the line spacing is a result of the combination of the interference between the electric field, the mechanical buckling of the jet and the stage movement error.

EHD patterning of the PEO solution is significantly influenced by the molecular weight of the polymer, the polymer concentrations, the driving voltage reduced from the threshold voltage, and the moving speed of the substrate. A single line whose width ranges from several tens of nm to several μm can be fabricated by selecting proper values for these process parameters. Furthermore, the line array as well as the grid pattern with 50-nm line width can also be readily obtained using the same process values.

CONCLUSION

We have suggested a systematic approach not only to improve the resolution of EHD direct patterning but also to reduce the applied electric field without using any mechanical assistance. EHD direct pattering of solutions from jet initiation to deposition on an ITO-coated glass was investigated with variations in several key parameters such as polymer concentration, molecular weight, driving voltage and moving speed of the substrate, in order to fabricate various straight patterns with a variety of line widths. There was little difference in the threshold voltage for the jet initiation among different solutions due to similar surface tensions. A very thin jet was obtained by reducing the driving voltage from the threshold voltage where a continuous jet was ejected when the viscosity was relatively high. The jet diameter was largely affected by the voltage reduction ratio as well as the polymer weight percent and molecular weight, which eventually was strongly associated with the mode of the resultant pattern on the substrate. For higher polymer weight percent and molecular weight, the pattern mode was transformed from beads-on-string to nanofibers due to the rapid solidification of the jet as the voltage reduction ratio was decreased. The resultant line patterns of 50 nm to 10 μm width were fabricated by controlling the moving speed of the substrate. Contour maps were also provided to show how the pattern mode transition occurs by changing the polymer weight percent, the molecular weight, and the voltage reduction ratio. Line arrays and grid pattern were also fabricated to demonstrate the feasibility of the proposed method. This work shows that PEO lines and grids with various widths from several tens of nm to several μm can be fabricated via EHD patterning, which is possible for printed electronics applications such as flexible sensors, solar cells, and nanogenerators.

ACKNOWLEDGEMENT

This research was supported by the Basic Science Research Program through the National Research Foundation of Korea (NRF) funded by the Ministry of Education (NRF-2013R1A1A2011800).

REFERENCES

1. A. Laforgue and L. Robitaille, *Macromolecules* 43, 4194 (2010).
2. Y.Z. Long, M.M. Li, C.Z. Gu, M.X. Wan, J.L. Duvail, Z.W. Liu, and Z.Y. Fan, *Prog. Polym. Sci.* 36, 1415 (2011).
3. A. Laforgue and L. Robitaille, *Synth. Met.* 158, 577 (2008).
4. S.Y. Min, T.S. Kim, B.J. Kim, H. Cho, Y.Y. Noh, H. Yang, J.H. Cho, and T.W. Lee, *Nat. Commun.* 4, 1773 (2013).
5. Y. Yuan, G. Giri, A.L. Ayzner, A.P. Zoombelt, S.C. Mannsfeld, J. Chen, D. Nordlund, M.F. Toney, J. Huang, and Z. Bao, *Nat. Commun.* 5, 3005 (2014).
6. C.E. Chang, V.H. Tran, J.B. Wang, Y.K. Fuh, and L.W. Lin, *Nano Lett.* 10, 726 (2010).
7. F.R. Fan, L. Lin, G. Zhu, W.Z. Wu, R. Zhang, and Z.L. Wang, *Nano Lett.* 12, 3109 (2012).
8. S.S. Yao and Y. Zhu, *Nanoscale* 6, 2345 (2014).
9. S. Nambiar and J.T.W. Yeow, *Biosens. Bioelectron.* 26, 1825 (2011).
10. X.X. Yang, B.W. Zhang, Z.Y. Liu, B. Deng, M. Yu, L.F. Li, H.Q. Jiang, and J.Y. Li, *J. Mater. Chem.* 21, 11908 (2011).
11. M.S. Mannoor, Z.W. Jiang, T. James, Y.L. Kong, K.A. Malatesta, W.O. Soboyejo, N. Verma, D.H. Gracias, and M.C. McAlpine, *Nano Lett.* 13, 2634 (2013).
12. D. Grafahrend, K.H. Heffels, M.V. Beer, P. Gasteier, M. Moller, G. Boehm, P.D. Dalton, and J. Groll, *Nat. Mater.* 10, 67 (2011).
13. B.J. Kang, C.K. Lee, and J.H. Oh, *Microelectron. Eng.* 97, 251 (2012).
14. D.J. Lee and J.H. Oh, *Thin Solid Films* 518, 6352 (2010).
15. C. Hellmann, J. Belardi, R. Dersch, A. Greiner, J.H. Wendorff, and S. Bahnmueller, *Polymer* 50, 1197 (2009).
16. C. Chang, K. Limkrailassiri, and L.W. Lin, *Appl. Phys. Lett.* 93, 123111 (2008).
17. N.B. Bu, Y.A. Huang, X.M. Wang, and Z.P. Yin, *Mater. Manuf. Process.* 27, 1318 (2012).
18. H.K. Choi, J.U. Park, O.O. Park, P.M. Ferreira, J.G. Georgiadis, and J.A. Rogers, *Appl. Phys. Lett.* 92, 123109 (2008).
19. J.U. Park, M. Hardy, S.J. Kang, K. Barton, K. Adair, D.K. Mukhopadhyay, C.Y. Lee, M.S. Strano, A.G. Alleyne, J.G. Georgiadis, P.M. Ferreira, and J.A. Rogers, *Nat. Mater.* 6, 782 (2007).
20. D.H. Reneker, A.L. Yarin, H. Fong, and S. Koombhongse, *J. Appl. Phys.* 87, 4531 (2000).
21. R.T. Collins, J.J. Jones, M.T. Harris, and O.A. Basaran, *Nat. Phys.* 4, 149 (2008).
22. M.M. Hohman, M. Shin, G. Rutledge, and M.P. Brenner, *Phys. Fluids* 13, 2201 (2001).
23. D.H. Reneker and A.L. Yarin, *Polymer* 49, 2387 (2008).
24. B.H. Cao and M.W. Kim, *Faraday Discuss.* 98, 245 (1994).
25. T. Han, D.H. Reneker, and A.L. Yarin, *Polymer* 48, 6064 (2007).
26. A.L. Yarin, S. Koombhongse, and D.H. Reneker, *J. Appl. Phys.* 89, 3018 (2001).